Towards a 3-D Technique to Determine the Geometric Path of Electric Current Flow Through a Contact System

Towards a 3-D Technique to Determine the Geometric Path of Electric Current Flow Through a Contact System

Constantinos C. Roussos and Jonathan Swingler

***Abstract*— The effective conductivity of a contact system is an important characteristic used to link the microstructure of the contact system to its performance. A resistor network model has been developed from the cross-sectional slices of a given electrical contact system. This allows the total resistance across the model and hence the total conductance of the system to be calculated. This resistor network model development is based on the contact interface, of the contact system, which is presented as a 3-D contact map. The 3-D contact map consists of contact spots that have been extended across the two bodies of the contact system as asperities. In this modeling process, a technique is developed that pictures any cross-sectional slice of the contact system and shows in which voxels the electric current flows. An X-ray computed tomography method is used to collect the data for visualizing the contact system and preparing the 3-D contact map. A 250-V, 16-A rated ac single-pole rocker switch is used as the contact system for investigation.**

***Index Terms*— Asperities, contact area, contact system, electrical contact, resistor network, X-ray computed tomography (CT).**

I. Introduction

THE electrical contact is an important component in many fields of engineering and sciences as it is an integral part of all electrical and microelectronic devices [1]–[7]. This component consists of two conductive surfaces brought together that allow an electric current to flow through it. The conductive surfaces of the bodies play an important role in the reliability of devices due to the contact normal force, material hardness, and surface roughness. The roughness of the surfaces causes a distribution of small peaks or asperities within the apparent area to be in mechanical and electrical contact.

The electrical area of contact can be visualized by many researchers using different methods [8]–[12]. More interesting studies in recent times are focused on nondestructive visualization methods involving magnetic resonance imaging [13], [14] and X-ray computed tomography (CT) [1], [10], [11], [15], [16]. These visualization methods offer the possibility to acquire 2-D and 3-D views of the samples without dismantling the component parts and destroying any features.

In previous work [1], X-ray CT is used to identify the contact spots that are in mechanical contact without dismantling the specimens and produce a "3-D contact map" of portion of areas of the electrical contact interface demonstrating the 3-D nature of the electrical contact. From the 3-D contact map, much information can be extracted such as the total area and the number of electrical contact spots [1], the distance between them [17], the area and the angle of each electrical contact spot [17], the total contact resistance, and the constriction resistance of each electrical contact spot [18]. Since the area of each electrical contact spot can be viewed at the micrometer scale, the mechanical and electrical properties at this microscale can be found, which vary significantly from bulk macroscale properties [1], [17]–[20].

In this paper, a resistor network model is constructed from data of a real contact system. This model is used to calculate the bulk or total resistance and hence the total conductance of the contact system. The network model is constructed from a 3-D contact map that identifies contact asperities across the conjoined two bodies of the contact system. The resistor network model can be used on any conductive contact system with nonuniform cross-sectional areas (perpendicular to the electric current direction), and each cross-sectional area can include more than one contact spot/asperity. Moreover, the simulated electric current in the model can flow in a nonuniform path through a contact system. (Each cross section across the contact interface has more than one contact spot, thus the amount of electric current flowing through each contact spot may be different.) An example is given in Fig. 1, which describes three cases of an electric current flowing through a contact system. In this example, it is assumed that the electric current flows through the whole cross-sectional area of Body A and passes to Body B through the contact interface.

Fig. 1(a) shows the contact system of two conductive bodies that are in mechanical contact at one point, and the cross-sectional area is the same at any point across the length (l) of two bodies. The total resistance (R) of a contact system with uniform cross section with a uniform flow of electric current (each cross section has no more than one electrical contact spot; thus, the amount of electric current flowing through each contact spot or cross-sectional area is equal) is

Manuscript received February 24, 2016; revised August 5, 2016 and April 28, 2017; accepted May 21, 2017. This work was supported in part by a DTA studentship funded by the U.K. Engineering and Physical Sciences Research Council (EPSRC) under Grant 1284817, in part by the National Institute of General Medical Sciences of the National Institutes of Health under Grant P41 GM103545-17, and in part by the DOE SciDAC Visualization and Analytics Center for Enabling Technologies under Grant DEFC0206ER25781. Recommended for publication by Associate Editor T. J. Schoepf upon evaluation of reviewers' comments. *(Corresponding author: Constantinos C. Roussos.)*

The authors are with the School of Engineering and Physical Sciences, Heriot-Watt University, Edinburgh EH14 4AS, U.K. (e-mail: c.roussos@cyi.ac.cy; j.swingler@hw.ac.uk).

Color versions of one or more of the figures in this paper are available online at http://ieeexplore.ieee.org.

Digital Object Identifier 10.1109/TCPMT.2017.2709541

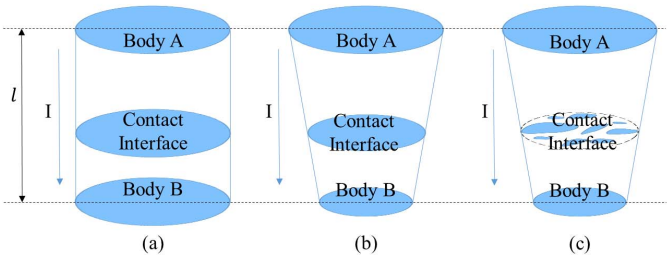

Fig. 1. Electric current flows through contact systems. Contact system with: (a) equal cross-sectional areas and one contact spot, (b) different sizes of cross-sectional areas and one contact spot, and (c) different sizes of cross-sectional areas and more than one contact spot.

given by,

$$R = \rho \frac{l}{A} \tag{1}$$

where ρ is the electrical resistivity and A is the cross-sectional area of the contact system.

Fig. 1(b) shows the contact system of two conductive bodies that are in mechanical contact at one point, and the cross-sectional area size has different values at any point across the length (l) of two bodies. The total resistance (R) of a contact system with nonuniform cross sections (each cross section has different size) with uniform flow of electric current (each cross section has no more than one electrical contact spot; thus, the amount of electric current flowing through each contact spot or cross-sectional area is equal) is given by

$$R = \rho \int_0^l \frac{1}{A(x)} dx. \tag{2}$$

This equation can also be used for the contact system of Fig. 1(a) as well.

The total resistance of the contact systems in Fig. 1(a) and (b) can be characterized as the sum of the series resistances. Each series resistance corresponds to the resistance of the cross-sectional area. When the contact system is in mechanical contact in more than one point as presented in Fig. 1(c), the calculation of the total resistance (R) of the contact system becomes nontrivial as the cross-sectional areas at the contact interface have many contact spots. These contact spots are connected in parallel, and their structures across the two bodies have different length dimensions. This is a result of the rough surfaces of the conductive bodies that are in mechanical contact.

Moreover, in this paper, the resistor network model is used in order to show the geometric path of electric current flowing through a contact system exhibiting multiple contact spots/asperities. Additionally, the total cross-sectional area of each cross-sectional slice (perpendicular on the electric current direction) is calculated and presented in comparison with the corresponding total cross-sectional area of each cross-sectional slice of electric current pathway. The number of asperities in each of these cross-sectional slices is also calculated and compared to the number of asperities through which the electric current flows.

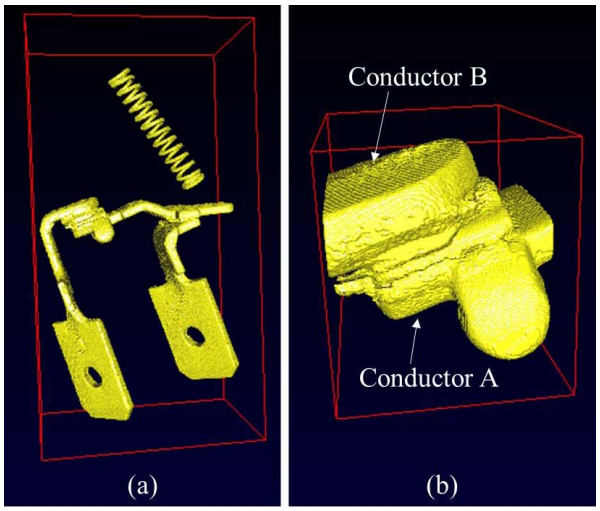

Fig. 2. Macrovisualizations. (a) Internal view of the single-pole rocker switch. (b) Close-up view of the volume of interest.

II. Experimental Methodology

A. Contact System Under Investigation and Macrovisualization

A 250-V, 16-A rated ac single-pole rocker switch with dimensions (3.5 × 2.5 × 3.0) cm is used as a contact system for investigation. The contact material is made of a silver alloy, while other conductors are made of a copper alloy. The internal view of the single-pole rocker switch is illustrated in Fig. 2(a). It consists of conductors and contact force spring. The geometry of the contact pair is a flat on flat with surface mean roughness, $R_a = 0.42 \pm 0.11$ μm for Conductor A and $R_a = 0.25 \pm 0.04$ μm for Conductor B. The surface roughness test was carried out using a contact profilometer Taylor Hobson RTH Talysurf 5-120 with a lateral x resolution of 0.1 μm and a height y resolution of 0.1 nm. The contact force is found to be 1.89 ± 0.07 N, and the bulk resistance across the contact pair was found to be $\sim$0.27 mΩ using the four-wire method. The close-up view of the contact pair, which is the volume of interest, is shown in Fig. 2(b).

B. Data Acquisition

For the data acquisition, an HMX 225 μCT system scanner is used. The system operates using an X-ray tomography designed by the XTek Group. The X-ray source is set to 175 kV, 133 μA, 23.28 W, which gives 3 μm focus capability.

The scanner rotates a sample through 360°, taking a series of 2-D X-ray images (2439 images are taken). The 2-D X-ray images are reconstructed as a 3-D source model using the "CT-Pro" software. This 3-D source model is used for all subsequent analysis of the data. The software "VGStudioMax" is then used to create 16-b 2-D cross-sectional slice images (791 images are taken) from the 3-D source model.

Fig. 3 shows an example of a 16-b 2-D cross-sectional slice image from a 250-V, 16-A ac single-pole switch. The various intensities of pixel illuminations are related to the level of X-ray absorption, which indicate different materials. The more highly absorbing silver alloy (lighter gray scale) is indicated with the less absorbing copper alloy metal, along

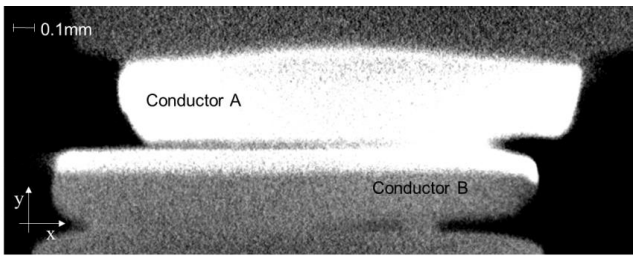

Fig. 3. 16-b cross-sectional slice image.

with the minimally absorbing air (black on the gray scale). The darker region between the two conductors is indicating air gaps.

These 16-b 2-D cross-sectional slice images are converted to 1-b images in order to separate the metal parts (white areas) of the contact system from the air (black areas) as explained in previous work [12]. In this paper, the 1-b 2-D cross-sectional slice images of the contact system are analyzed with contact analysis techniques (CAT). These CAT are developed and implemented with a suite of tools developed in MATLAB and Image Processing Toolbox in order to build the resistor network model of the contact system.

III. Contact Analysis and Modeling Techniques

A. Concept and Characteristics of a Resistor Network Model System

The calculation of the electric current pathways through a contact system requires knowledge of the distribution of the contact material constituents and their conductivities, as well as the size distribution of the contact asperities at the interface. In this paper, it is assumed that the contact system is made of the same material to simplify the resistor network model. The 2-D cross-sectional slice images in the *xy*- and *xz*-directions are extracted from the oriented 3-D volume of interest of the contact system. It is this resistor network model that is used to determine the current pathways. The method consists of different techniques that are given in Section III-B. For the resistor network model development, a similar method used to calculate the electrical resistance of a contact system [(2)] is used. Fig. 4(a) illustrates a schematic oriented 3-D volume of interest of a contact system, which is used in order to explain this method. It consists of two rough bodies, A and B, that are in mechanical contact. The mechanical contact occurs at the two constriction asperities [groups of gray voxels in Fig. 4(a)]. In this research, the structures of these constriction asperities above and below the two bodies of the schematic oriented 3-D volume of interest of a contact system are called contact asperities. The roughness of two bodies, where their "peaks" are not in mechanical contact, are called noncontact asperities. The schematic oriented 3-D volume of interest of a contact system of Fig. 4(a) consists of two contact asperities and five noncontact asperities. These asperities (contact asperities and noncontact asperities) are illustrated in Fig. 4(b) and (c), respectively.

B. Development of Open/Closed and Closed Resistor Network Models

First of all, the contact system is required to be divided into equal *x*-*z* cross-sectional slices across the electric current (I) direction (y-direction). The electric current direction is defined to be parallel with the normal force (F), and it is assumed that it flows through the whole cross-sectional area of the first and last *x*-*z* cross-sectional slices. The direction of the normal force is used to define the orientation of the coordinate system used. The schematic contact system of Fig. 4(a) consists of six *x*-*z* cross-sectional slices, and the second is illustrated in Fig. 4(d). The *x*-*z* cross-sectional slices consist of slice asperity, or slice asperities. A slice asperity is defined as a collection of voxels that are neighboring other voxels by at least one point of their edges. For example, the *x*-*z* cross-sectional slice of Fig. 4(d) has four slice asperities.

Fig. 5(b) shows the resistor network of the schematic oriented 3-D volume of interest of the contact system of Fig. 5(a) [same as Fig. 4(a)]. Each resistor R_{i_j} (where the suffixes i and j represent the cross-sectional slice and the resistor/slice asperity numbers, respectively) corresponds to a slice asperity on each *x*-*z* cross-sectional slice. For example, the *x*-*z* cross-sectional slice of Fig. 4(d) has four slice asperities or resistors where their values are given by (1), in which the length l in y-direction equals the resolution of the X-ray CT technique (5 μm in this paper). It is important to note that all the slice asperities or resistors have the same length l (y-direction), while their shapes (xz-direction) and cross-sectional sizes vary.

Fig. 5 shows the schematic oriented 3-D volume of interest of a contact system with its resistor network, where the blue slice asperities (groups of blue voxels in each *x*-*z* cross-sectional slice) are connected to open circuits, while the red slice asperities (groups of red voxels in each *x*-*z* cross-sectional slice) are connected to closed circuits. To show the geometric pathway of electric current flow through the contact system of Fig. 5, a potential difference across the two bodies is applied. It is obvious that the current flows only through the slice asperities or resistors that are connected to the network as a closed circuit as illustrated in Fig. 6(a) [and Fig. 6(b)]. To show the geometric pathways of electric current flow through the contact system of Fig. 5(a), it is required to modify the *x*-*z* cross-sectional slices of it in order to present only the slice asperities (or resistors), which the current flows through like the contact system of Fig. 6(a) and the resistor network of Fig. 6(b). For these modifications, three CAT are used.

The first technique is to develop the 3-D constriction asperities map using the CAT for Asperities (CATA), which gives information on where the electrical constriction asperities in a 3-D volume profile are located. CATA shows that the electric current flows through the 3-D constriction asperities [18]. This technique is a continuation of the 3-D contact maps developed in [1] and extended by one voxel in the electric current direction as presented in [18] as 3-D constriction asperities maps. Fig. 7(a) illustrates the 3-D constriction asperities map of the schematic oriented 3-D volume of interest of the contact system of Fig. 5(a).

The second technique is the CAT for contact voxels (CATV). This technique is used to create an *x*-*z* contact slice with all the constriction asperities at the same height (y-direction) as illustrated in Fig. 7(b). As mentioned before, the electric current flows through the 3-D constriction asper-

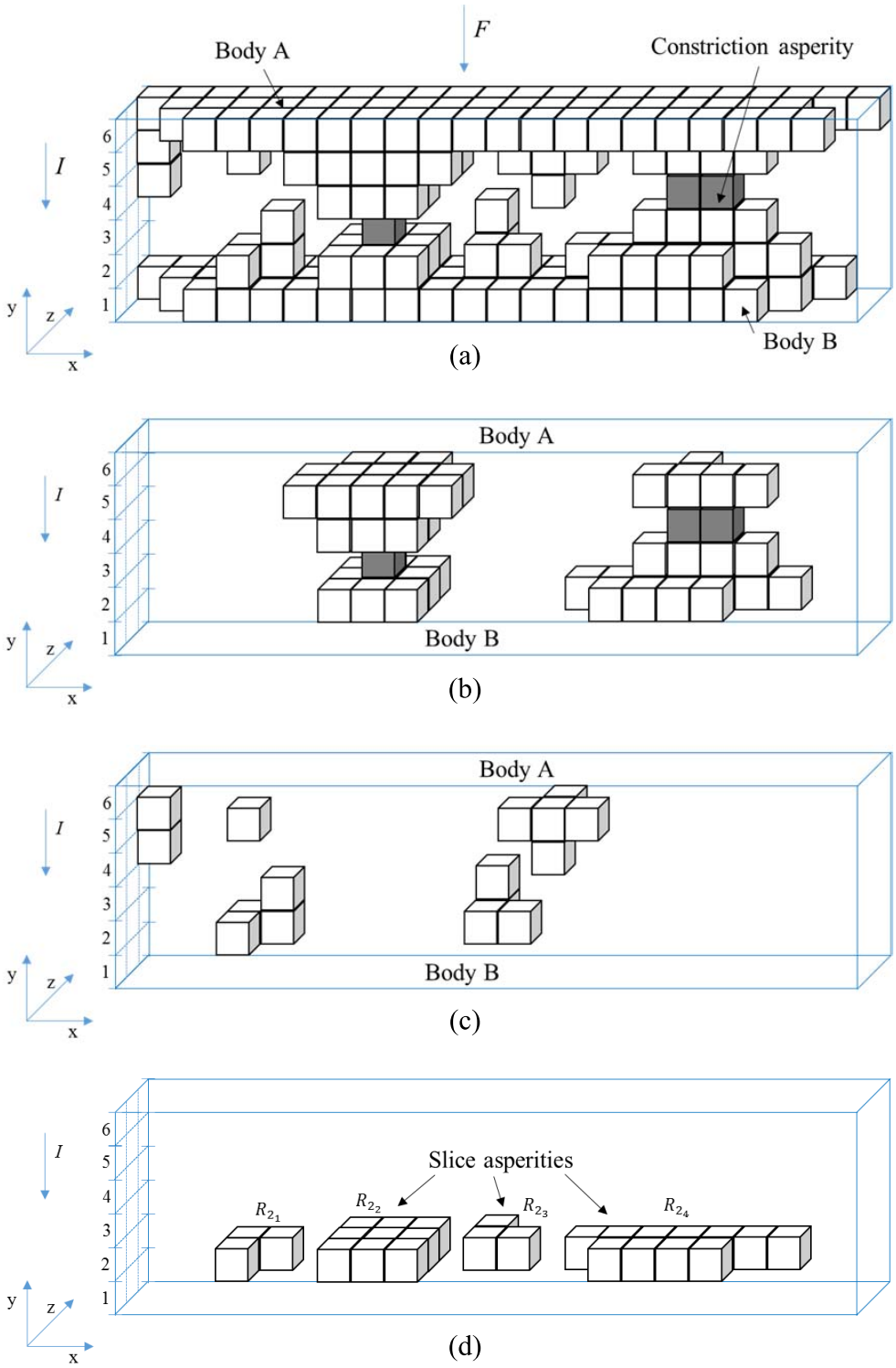

Fig. 4. Schematic contact system with its characteristics. (a) Schematic oriented 3-D volume of interest. (b) Contact asperities. (c) Noncontact asperities. (d) Second $x - z$ cross-section slice.

ities, and consequently, it flows through the x-z contact slice.

The third technique, CAT for comparison (CATC) is developed in order to compare each x-z cross-sectional slice to the x-z contact slice. The reason for making a comparison is to identify which of the slice asperities of x-z cross-sectional slice are connected with any of the constriction asperities of x-z contact slice. If there is a connection between the slice asperity j of x-z cross-sectional slice and any of the constriction asperities in x-z contact slice, then the electric current flows through the slice asperity j, of x-z cross-sectional slice.

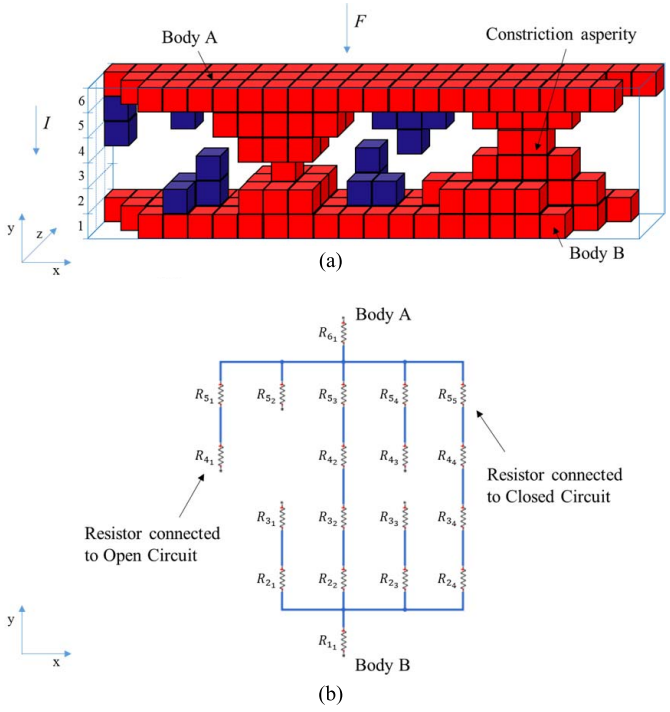

Fig. 5. Schematic oriented 3-D volume of interest of contact system with its resistor network. (a) Schematic oriented 3-D volume of interest. (b) Resistor network (open/closed circuit).

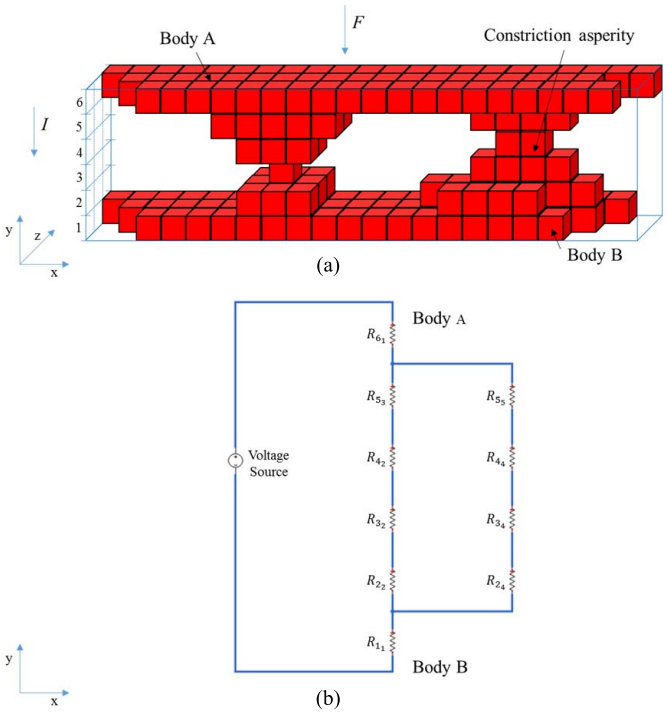

Fig. 6. Schematic 3-D contact source model of (a) schematic oriented 3-D volume of interest of contact system with (b) its resistor network.

If there is no connection between the slice asperity j of x-z cross-sectional slice and any of the constriction asperities in x-z contact slice, then the electric current does not flow through the slice asperity j and this slice asperity is removed from x-z cross-sectional slice. A mathematical example of this technique is given below describing the geometric path of electric current flows through the schematic oriented 3-D volume of interest of contact system of Fig. 5(a).

The matrix $[A]$ of (3), as shown at the bottom of this page, represents the x-z contact slice of Fig. 7(b), where zeros and α elements of matrix $[A]$ represent voxels with air and solids of the schematic oriented 3-D volume of interest of the contact system, respectively. A constriction asperity is defined as a collection of solid voxels that are neighboring other solid voxels by at least one of their edges. The matrix $[A]$ or the x-z contact slice consists of two constriction asperities.

Matrix $[B_{i_j}]$ represents the x-z cross-sectional slice for $i \in [1, N]$ and $j \in [1, S]$, where i is the number of x-z cross-sectional slice, N is the total number of x-z cross-sectional slices, j is the number of the slice asperity, and S is the total number of the slice asperities within the x-z cross-sectional slice. Zeros and β elements of matrix $[B_{i_j}]$ represent voxels with air and solids of the schematic oriented 3-D volume of interest of the contact system, respectively. The matrix $[B_2]$ or the second x-z cross-sectional slice of Fig. 6(a)

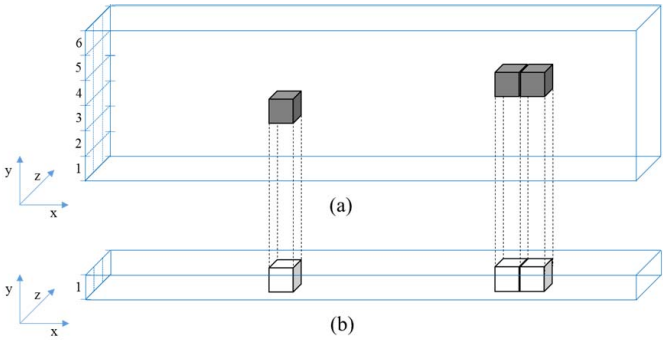

Fig. 7. (a) 3-D constriction asperities map. (b) x-z contact slice.

consists of four slice asperities. The matrices of (4) and (5), as shown at the bottom of the next page, represent the first and second slice asperities of the second x-z cross-sectional slice, respectively

Comparing whether there is a connection between the first ($j = 1$) slice asperity of the second ($i = 2$) x-z cross-sectional slice and any of the constriction asperities in x-z contact slice, (3) and (4) are added as presented in (6), as shown at the bottom of the next page. The comparison of the second ($j = 2$) slice asperity of the second ($i = 2$) x-z cross-sectional slice with any of the contact asperities in x-z contact slice is also presented as described in (7), as

$$[A] = \begin{bmatrix} 0 & 0 & 0 & 0 & 0 & 0 & 0 & 0 & 0 & 0 & 0 & 0 & 0 & 0 & 0 & 0 & 0 & 0 & 0 & 0 & 0 & 0 \\ 0 & 0 & 0 & 0 & 0 & 0 & 0 & \alpha & 0 & 0 & 0 & 0 & 0 & 0 & 0 & 0 & \alpha & \alpha & 0 & 0 & 0 & 0 \\ 0 & 0 & 0 & 0 & 0 & 0 & 0 & 0 & 0 & 0 & 0 & 0 & 0 & 0 & 0 & 0 & 0 & 0 & 0 & 0 & 0 & 0 \end{bmatrix} \tag{3}$$

shown at the bottom of this page. The matrix $[C_{i_j}]$ is the sum of matrix $[A]$ with matrix $[B_{i_j}]$. The γ element represents the summation of α and β elements and shows if there is a connection between the slice asperity j of i x-z cross-sectional slice and any of the constriction asperities in x-z contact slice. The same procedure is used for the rest of the slice asperities of the second x-z cross-sectional slice

Each of the slice asperities presented in the matrix $[C_{i_j}]$ is examined separately in order to identify whether the electric current flows through it or not. If the electric current flows through a slice asperity, the γ element is included within the slice asperity and a new matrix $[D_{i_j}]$ is created that contains only this slice asperity, which is renamed with the δ elements. This condition is described by the matrix of (9), as shown at the bottom of this page. A slice asperity without the γ element is replaced with zeros as described by the matrix of (8), as shown at the bottom of this page. The same procedure is used for the rest of the slice asperities of the second x-z cross-sectional slice

The last matrix is created in order to include all the slice asperities of the slice where the electric current flows through them and is described by

$$[E_i] = \sum_{j=1}^{S} [D_{i_j}]. \tag{10}$$

(S is the total number of the slice asperities within the x-z cross-sectional slice.) The final matrix of the second x-z cross-sectional slice of the schematic oriented 3-D volume of interest of contact system of Fig. 5(a) is given by (11), as shown at the bottom of this page. The same procedure, used in second x-z cross-sectional slice, is used for the rest of x-z cross-sectional slices.

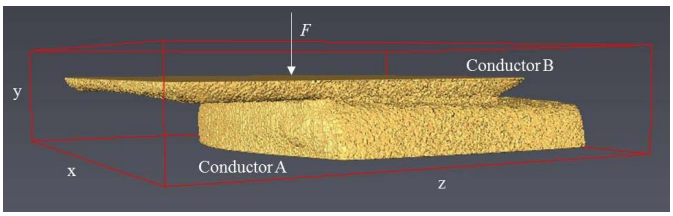

Fig. 8. 3-D source model of the 250-V, 16-A rated ac single-pole rocker switch with bounding box dimensions of 3.22 × 0.71 × 3.31 mm.

The geometric path of electric current flow through a contact system consists of all the processed x-z cross-sectional slices in a 3-D plane. The result of this procedure is called 3-D contact source model. For example, the schematic oriented 3-D volume of interest of Fig. 5(a) is illustrated in Fig. 6(a), which consists of the red voxels only. The noncontact asperities (groups of blue voxels) are removed from the oriented 3-D volume of interest because they are connected to open circuits. (The electric current is not flowing through the open circuits when a voltage is applied).

IV. Results And Analysis

A. Contact System

Fig. 8 shows a part of the 3-D volume of interest of the contact system of the switch that is labeled as the 3-D source model. This part of volume is selected from the 3-D volume of interest of Fig. 2(b) that is oriented so that its normal force (F) could be parallel with y-axis. (The reason of orientation is explained in Section III-B.) More details concerning the selection of this part of volume (3-D source

$$[B_{2_1}] = \begin{bmatrix} 0&0&0&0&0&0&0&0&0&0&0&0&0&0&0&0&0&0&0&0&0&0 \\ 0&0&0&\beta&\beta&0&0&0&0&0&0&0&0&0&0&0&0&0&0&0&0&0 \\ 0&0&0&\beta&0&0&0&0&0&0&0&0&0&0&0&0&0&0&0&0&0&0 \end{bmatrix} \tag{4}$$

$$[B_{2_2}] = \begin{bmatrix} 0&0&0&0&0&0&\beta&\beta&\beta&0&0&0&0&0&0&0&0&0&0&0&0&0 \\ 0&0&0&0&0&0&\beta&\beta&\beta&0&0&0&0&0&0&0&0&0&0&0&0&0 \\ 0&0&0&0&0&0&\beta&\beta&\beta&0&0&0&0&0&0&0&0&0&0&0&0&0 \end{bmatrix} \tag{5}$$

$$[C_{2_1}] = \begin{bmatrix} 0&0&0&0&0&0&0&0&0&0&0&0&0&0&0&0&0&0&0&0&0&0 \\ 0&0&0&\beta&\beta&0&0&\alpha&0&0&0&0&0&0&0&0&\alpha&\alpha&0&0&0&0 \\ 0&0&0&\beta&0&0&0&0&0&0&0&0&0&0&0&0&0&0&0&0&0&0 \end{bmatrix} \tag{6}$$

$$[C_{2_2}] = \begin{bmatrix} 0&0&0&0&0&0&\beta&\beta&\beta&0&0&0&0&0&0&0&0&0&0&0&0&0 \\ 0&0&0&0&0&0&\beta&\gamma&\beta&0&0&0&0&0&0&0&\alpha&\alpha&0&0&0&0 \\ 0&0&0&0&0&0&\beta&\beta&\beta&0&0&0&0&0&0&0&0&0&0&0&0&0 \end{bmatrix} \tag{7}$$

$$[D_{2_1}] = \begin{bmatrix} 0&0&0&0&0&0&0&0&0&0&0&0&0&0&0&0&0&0&0&0&0&0 \\ 0&0&0&0&0&0&0&0&0&0&0&0&0&0&0&0&0&0&0&0&0&0 \\ 0&0&0&0&0&0&0&0&0&0&0&0&0&0&0&0&0&0&0&0&0&0 \end{bmatrix} \tag{8}$$

$$[D_{2_2}] = \begin{bmatrix} 0&0&0&0&0&0&\delta&\delta&\delta&0&0&0&0&0&0&0&0&0&0&0&0&0 \\ 0&0&0&0&0&0&\delta&\delta&\delta&0&0&0&0&0&0&0&0&0&0&0&0&0 \\ 0&0&0&0&0&0&\delta&\delta&\delta&0&0&0&0&0&0&0&0&0&0&0&0&0 \end{bmatrix} \tag{9}$$

$$[E_2] = \begin{bmatrix} 0&0&0&0&0&0&\delta&\delta&\delta&0&0&0&0&0&0&0&0&0&0&0&0&0 \\ 0&0&0&0&0&0&\delta&\delta&\delta&0&0&0&0&\delta&\delta&\delta&\delta&\delta&\delta&\delta&0&0 \\ 0&0&0&0&0&0&\delta&\delta&\delta&0&0&0&0&0&\delta&\delta&\delta&\delta&0&0&0&0 \end{bmatrix} \tag{11}$$

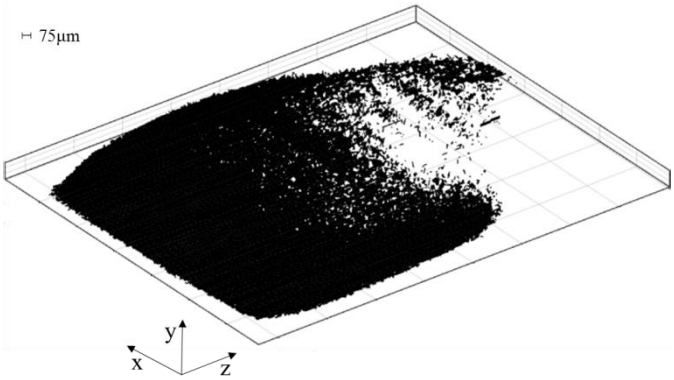

Fig. 9. 3-D contact map.

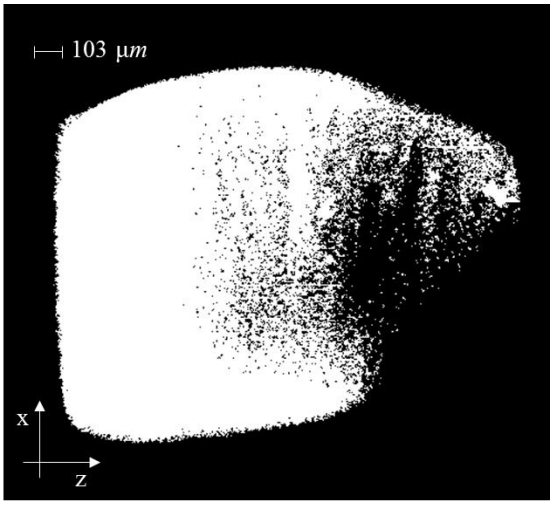

Fig. 10. 2-D contact map.

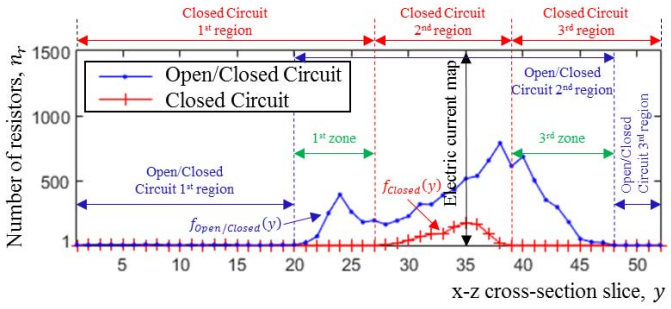

Fig. 11. Number of resistors in each *x-z* cross-sectional slice image of the 3-D source model for open/closed circuit and closed circuits.

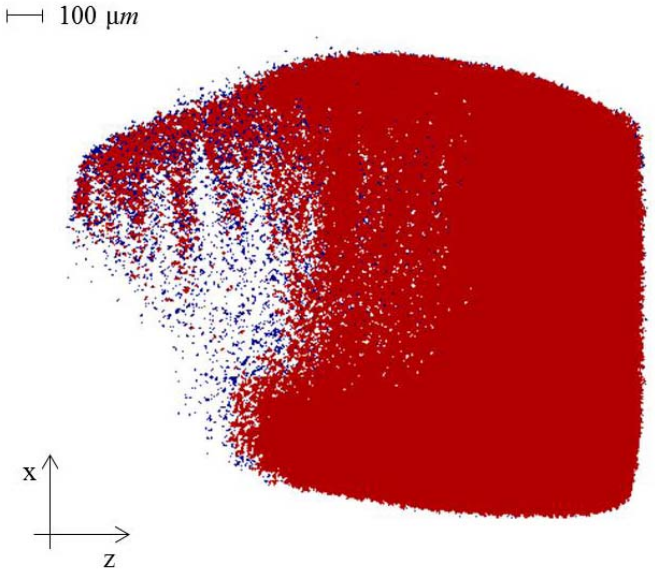

Fig. 12. Cross-sectional area of the 35th *x-z* cross-sectional slice of the 3-D source model.

model) from the 3-D volume of interest of Fig. 2(b) are given in Section V-B.

B. 2-D and 3-D Contact Maps

Fig. 9 illustrates the 3-D contact map of the contacting interface between the conductors of the 3-D source model of the switch. The 3-D contact map is visualized using the 2-D cross-sectional slice images that are processed and implemented using CAT with a suite of tools developed in MATLAB as described in [1]. The 3-D contact map consists of contact spots (pixels, surfaces) that are the cross-sectional areas of the constriction asperities (voxels, volumes). Fig. 10 illustrates the 2-D cross-sectional of *x-z* contact slice of the 3-D source model of the switch. The *x-z* contact slice is developed using CATV in order to set all the contact spots of the 3-D contact map of Fig. 9 to the same height.

C. Resistor Network Model of the Contact System

Fig. 11 shows the graph of number of resistors in each *x-z* cross-sectional slice of the 3-D source model (as explained in Section IV-A) and the 3-D contact source model (the processed *x-z* cross-sectional slice images of the 3-D source model as explained in Section III-B) of the switch. Each resistor represents a slice asperity in the *x-z* cross-sectional slice. The graphs are separated as open/closed-circuit (3-D source model) and closed circuit (3-D contact source model), which present the number of resistors that make up the open/closed circuit or closed circuit. The graph presented in Fig. 11 is divided into regions and zones. The reason for this division is explained in detail in Section V. If voltage is applied, the current will flow through the closed circuit. The closed-circuit resistor network model (the *x-z* cross-sectional slice images of the 3-D contact source model) shows exactly where the current will flow and its magnitude.

D. Electric Current Path Map

Fig. 12 illustrates the electric current path map (or electric current map) of the 3-D source model of the switch. In this paper, an electric current map is defined by the *x-z* cross-sectional slice of the 3-D source model (open/closed circuit) with the largest number of resistors that are connected to closed circuits. For example, the electric current map of the 3-D source model (open/closed circuit) in Fig. 12 is the 35th *x-z* cross-sectional slice. This 35th *x-z* cross-sectional

slice has the largest number of resistors in the closed circuit. When a simulated potential difference is applied across the 3-D source model, an electric current will flow through it. The red areas of electric current map present the areas that are affected by electric current. The geometric path of electric current that flows through these red areas of the electric map of the 3-D source model is presented with the red color. The blue areas present the areas where the electric current is not flowing through them, while white areas indicate voids.

E. Total Cross-Sectional Area of Slice Asperities

The cross-sectional area of a slice asperity is defined as the sum of pixels within the slice asperity. The sum of the cross-sectional area of slice asperities in each *x-z* cross-sectional slice gives the total cross-sectional area of the *x-z* cross-sectional slice. Fig. 13 shows the graph of the total cross-sectional area in each *x-z* cross-sectional slice of the 3-D source model and the 3-D contact source model of the switch. The graph is separated as closed-circuit (3-D contact source model) and open/closed-circuit (3-D source model), which presents the areas that are affected (electric current flows through them) when a simulated potential difference is applied, or not, across the two conductors of the 3-D source model.

V. Discussion

A. X-ray CT Method

The results show that the X-ray CT is a powerful method for viewing the contact interface of a contact system without needing to dismantle it. The data acquired using this method with voxel resolution of 5 μm $\times$ 5 μm $\times$ 5 μm give the ability of examination and processing in order to investigate different characteristics that occur in a contact interface and its extension. These characteristics include the total area and the number of electrical contact spots [1], the distance between them [17], the area and angle of each electrical contact spot [17], the total contact resistance, and the constriction resistance of each electrical contact spot [18]. Moreover, these characteristics include the development of resistor network model of a given contact system that is introduced in this paper in order to determine its effective conductance showing the geometric path of electric current that flows through of any cross-sectional slice.

The resolution is a very important factor for the calculation and visualization methods. For example, for a coarse measurement (e.g., 100 μm) of resolution, only a few asperities of large curvature are visualized, while for smaller measurement (e.g., 0.1 μm) of resolution, more asperities of smaller curvature are visualized [20], [21]. The smallest resolution that can be obtained by the current facility is 3 μm. This depends on the sample dimensions and X-ray admittance of the sample materials. The resolution of 5 μm obtained in this paper is the optimum that could be achieved with the sample configuration used. However, it should be noted that the CAT developed and implemented within a suite of tools in this paper can be used with data of smaller resolution.

B. Contact Analysis Techniques

Analysis and modeling techniques are developed to build the resistor network model of a given contact system in order to determine its effective conductance showing the geometrical path of electric current that flows through any cross-sectional slice. These techniques (CATA, CATV, and CATC) are developed in MATLAB using Image Processing Toolbox, and their general method is based on (2).

The selection of the 52 *x-z* cross-sectional slices that compose the contact system of Fig. 8 is based on their 16-b grayscale values. As mentioned in Section II-B, the various intensities of pixel illuminations related to the level of X-ray absorption indicate different materials of the voxel, thus different resistivities. These 52 *x-z* cross-sectional slices are from the lighter area of the 16-b *x-y* cross-sectional slice of Fig. 3, which are then converted into 1-b slice image as it is assumed that the slice asperities have the same resistivity. Each slice asperity in the *x-z* cross-sectional slice corresponds with a spot in 2-D *x-z* cross-sectional slice image and with a resistor in the resistor network model.

In previous work [1], [18], it is reported that the electric current flows through the contact interface, which is visualized as a 3-D contact map. According to this, the 3-D contact map as presented in Fig. 9 of the contact system of Fig. 8 is converted into a 2-D contact map as presented in Fig. 10. The 2-D contact map is used as the reference *x-z* contact slice to make a comparison to each *x-z* cross-sectional slice of the contact system as described in Section III-B. This comparison is made in order to investigate from which spots of the *x-z* cross-sectional slice the electric current flows through. It is important to mention that 2-D contact maps are also developed by Lalechos and Swingler [10] and Lalechos *et al.* [19] using a different method. The differences of these methods are given in previous work [1].

C. Resistor Network Model of the Contact System Findings

The resistor network model is developed based on the separation of voxels into slice asperities, according to which a slice asperity of a contact system corresponds with a resistor in the resistor network model. For the calculations of the resistor network model, the resistor network model is separated as open/closed circuit (when no voltage applied) and closed circuit (when voltage applied). The open/closed-circuit resistor network model is referred when a potential difference does not apply to it and its resistors correspond to the slice asperities of nonprocessed *x-z* cross-sectional slices. The closed-circuit resistor network model is referred when a potential difference applies on it and its resistors correspond to the slice asperities of processed *x-z* cross-sectional slices.

The graphs of closed circuit and open/closed circuit of the resistor network model in Fig. 11 show that the resistors follow different distribution. The graph of the open/closed-circuit resistor network model consists of minima and maxima at many points across the region of contact. According to the graph of the open/closed-circuit resistor network model in Fig. 11, the resistor network model can be divided into three main regions. The limits of each of these three main

regions are given on the graph of Fig. 11. Each *x-z* cross-sectional slice image of the first and third region consists of only one slice asperity (resistor). According to (2), the resistors of the first and third regions are connected in series as each *x-z* cross-sectional slice image has only one resistor. The resistors at the second region are connected intricately in closed and open circuits [see Fig. 5(b)], making the calculation of the total resistance in the region difficult and complicated. This region is the result of the roughness of two conductors of the contact system in the contact section.

More interest is focused on the closed-circuit resistor network model, as this includes only the resistors where the electric current flows through them. Compared to the open/closed-circuit resistor network model, the closed-circuit resistor network includes only the resistors that are connected to closed-circuits [see Fig. 6(b)]. The graph of closed-circuit resistor network model of Fig. 11 consists of a maximum in the contact section (second region). The *x-z* cross-sectional slice image with the largest number of resistors in closed-circuit resistor network model is labeled as the electric current map. The total number of resistors within these *x-z* cross-sectional slice images (or electric current maps) is also included for both resistor network models (open/closed circuit and closed circuit). More details concerning the electric contact maps are given in Section V-E. According to the graph of the closed-circuit resistor network model in Fig. 11, the resistor network model can be divided into three main regions. The limits of each of these three main regions are given in the graph of Fig. 11. Each *x-z* cross-sectional slice image of the first and third region consists of only one slice asperity (resistor). According to (2), the resistors of the first and third regions are connected in series as each *x-z* cross-sectional slice image has only one resistor. The resistors at the second region are connected intricately, making the calculation of the total resistance in the region difficult and complicated (but easier compared to the second region of open/closed-circuit resistor network). This region corresponds to the roughness of two conductors of the contact system. Moreover, Fig. 11 shows that as the cross-sectional slices of the closed-circuit resistor network tend to the contact region, the total number of their resistors (slice asperities) increases.

D. Total Resistance of the Contact System

The total resistance across the contact system is given from the sum of total resistance in each region. The closed-circuit resistor network model that is introduced in this paper will be used in order to calculate the total resistance across conductors of the switch and hence the total conductance of it. The open/closed-circuit resistor network model is excluded as the open circuits do not affect the total values of the resistance and conductance.

Table I illustrates the total resistance and conductance of the first zone, second region, and third zone as well as the total resistance and conductance across the first and third zone of the 3-D contact source model (closed-circuit resistor network model) of the switch. The limits of the second region of open/closed-circuit resistor network model are the same with the limits between the first and third zones of the contact

TABLE I

RESISTANCE AND CONDUCTANCE VALUES IN EACH ZONE AND THEIR TOTAL VALUES ACROSS THE FIRST AND THIRD ZONE OF THE 3-D CONTACT SOURCE MODEL

	Resistance ($n\Omega$)	Conductance (MS)
1st zone	151.89	6.58
2nd region	336.02	2.98
3rd zone	155.58	6.43
Total	643.49	1.55

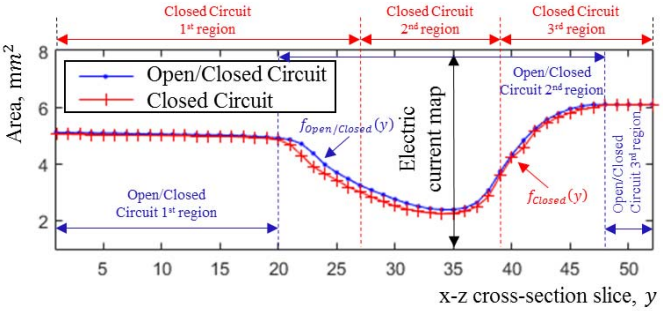

Fig. 13. Total cross-sectional area in each *x-z* cross-sectional slice image of the 3-D source model for open/closed and closed circuits.

system (see Fig. 11). The first zone in the graphs of Fig. 11 is defined by the common *x-z* cross-sectional slices between the first region of the closed circuit and the second region of the open/closed circuit. The third zone in the graphs of Fig. 11 is defined as the common *x-z* cross-sectional slices between the third region of the closed circuit and the second region of the open/closed circuit. These zones (first and third) are defined in order to illustrate an example of resistance and conductance calculations across the second region of open/closed-circuit resistor network model.

The total resistance of the first and third zone in Table I is calculated by adding the resistance of each *x-z* cross-sectional slice image of the 3-D contact source model (closed circuit) using (1). The resistance of each *x-z* cross-sectional slice (of first and third zone) is calculated by using the total mechanical area of contact in each *x-z* cross-sectional slice image. The total mechanical area of contact of each *x-z* cross-sectional slice image is given in Fig. 13 (the closed-circuit values), where the length l in y-direction and electrical resistivity (of silver) ρ of (1) are equal to 5 μm (length of voxel) and 15.87×10^{-9} Ωm, respectively. The conductance is given from the inverse value of resistance.

The resistance across the second region is difficult to calculate due to the intricate connections of the resistors at the region. However, an approach is introduced in this

research by modifying Greenwood's formula, which is given from [4]

$$R = \frac{\rho}{2\sum a_i} + \frac{\rho}{\pi(\sum a_i)^2} \sum\sum_{i \neq j} \frac{a_i a_j}{d_{ij}}. \quad (12)$$

This gives the total contact resistance, which depends on the distances between the set of circular contact spots (the formula is based on electrostatics [22]). According to this, (12) applies to surfaces (contact spots). The modification on (12) that is given from (13) is made in order to apply in volumes (slice asperities)

$$R = \frac{\rho \cdot l}{\sum A_i} + \frac{\rho}{\pi(\sum a_i)^2} \sum\sum_{i \neq j} \frac{a_i a_j}{d_{ij}}. \quad (13)$$

It is important to note that the potential difference across each slice asperity (resistor) in the x-z cross-sectional slice is assumed to be equal with the other slice asperities (resistors) in the x-z cross-sectional slice of the 3-D contact source model (closed-circuit resistor network).

Equation (13) gives the total resistance for each x-z slice on the second region of Closed Circuit (see Fig. 11) resistor network model of the 3-D contact source model. To achieve this, the cross-sectional area of each slice asperity in the y-direction is assumed to be a circle of radius α. For example, the radius of contact spot i is calculated by (14)

$$a_i = \sqrt{\frac{A_i}{\pi}} \quad (14)$$

where A_i is the total cross-sectional area of slice asperity i. The distance d_{ij} between slice asperity i and j is calculated from the centroids of slice asperities i and j, where the length l in y-direction and electrical resistivity (of silver) ρ of (13) are equal to 5 μm (length of voxel) and 15.87×10^{-9} Ωm, respectively. The total resistance of the second region after each current loading test presented in Table I is calculated by adding the total resistance of each x-z slice of the closed-circuit (see Fig. 11) resistor network model of the 3-D contact source model. The total conductance is given from the inverse value of total resistance.

The total resistance value in Table I is calculated by adding the total resistance of the first zone, second region, and third zone. This value of the resistance (643.49 nΩ) corresponds to 0.26 mm length (52 x-z cross-sectional slices $\times$ 5 μm). In order to investigate if this calculated value of the resistance corresponds to the reality, a four-wire method was applied by applying the voltage probes very close to the contact area of the switch. The value of the resistance using the four-wire method is measured to be 3100 nΩ, which corresponds to 1.07 mm length (the distance between the voltage probes of the four-wire method). Comparing the measured value (3100 nΩ) to the calculated value (643.49 nΩ) of the resistance, it is obvious that the measured value is larger. This was expected because the two values of the resistance correspond to different lengths [when the length of the material is increasing, the resistance is increasing too; see (1)].

Ideally, to prove that the measured value of the resistance equals at the corresponding length of calculated value of the resistance, the ratio of the lengths and the ratio of the resistances (measured and calculated) should be equal. This proof matches perfectly in case the sample describes the contact system of Fig. 1(a). However, this proof is used in the case of the switch. In this condition, the ratio of the lengths and the ratio of the resistances of the measured and calculated values of the switch are found to be 0.243 and 0.208, respectively. Comparing the two ratios, it is obvious that they have 14.4% difference. This difference was expected because the switch describes the contact system of Fig. 1(c), where its cross sections have different shapes and sizes and its contact interface has many contact spots of different shapes and sizes as well.

Additionally, there are two more factors that justify the difference of 14.4% between the measured and calculated values. The first one is due to different materials that make the two conductors of the contact system, the silver alloy and copper alloy. The resistance that is measured using the four-wire method across the two conductors of the contact system considers all the materials. These materials (silver alloy and copper alloy) have different electrical resistivities resulting in the bulk resistance in copper alloy regions to be bigger as the copper alloy has a larger electrical resistivity compared to silver alloy (this value is included to 3100 nΩ of resistance). The second one is due to the inability of the technique (calculation method) to identify and make the appropriate calculations at the contact areas that have been oxidized and corroded [23]–[25]. This factor is very crucial for the calculation of the contact resistance and, by extension, the value of the calculated resistance.

E. Electric Current Map Findings

The cross-sectional area of the 35th x-z cross-sectional slice of the 3-D source model (open/closed circuit) of the switch is illustrated in Fig. 12, which shows its resistors (red and blue spots). The blue and red spots (514 in number) show the resistors of the open/closed-circuit resistor network model. The red spots (171 in number) show the resistors of the closed-circuit resistor network model and the geometric path of electric current that flows through the voxels of the 35th x-z cross-sectional slice of the 3-D source model.

F. Total Cross-Sectional Area of Slice Asperities Findings

The cross-sectional area of each x-z cross-sectional slice of the 3-D source model (open/closed circuit) of the switch is calculated counting the number of voxels in each slice and multiplied with the pixel size (5 μm $\times$ 5 μm). The cross-sectional area of each x-z cross-sectional slice for both (open/closed-circuit and closed-circuit) resistor network models is given in Fig. 13. The graphs of Fig. 13 show that the cross-sectional areas of both (open/closed-circuit and closed-circuit) resistor network models follow similar distributions. The smallest cross-sectional areas appear on the 34th x-z cross-sectional slice (for both, open/closed and closed circuits) with 2.39 mm^2 for the open/closed-circuit resistor network model and 2.25 mm^2 for the closed-circuit resistor network model. Moreover, it is important to note that the graphs of Fig. 13 show that as the cross-sectional slices tend

to the contact region, the total cross-sectional area of the cross-sectional slice decreases. This indicates that as the cross-sectional slices tend to the contact region, the total volume of their resistors (slice asperities) decreases.

VI. Conclusion

The X-ray CT method is used in order to visualize the contact system of a single-pole rocker switch without the need to dismantle the sample. A resistor network model of a contact system is developed and introduced based on the slice asperities of the cross-sectional slice images. These slice asperities consist of voxel or voxels that represent the 3-D microstructures of the contact system. The cross-sectional slice images of the contact system that are acquired from the X-ray CT are processed using CAT, which are developed and implemented with a suite of tools developed in MATLAB and Image Processing Toolbox. These techniques can be used for any contact system for any value of resolution.

The resistor network model is found to demonstrate that the contact system at the restriction zone consists of open and closed circuits. In the modeling process, a technique that is presented in this paper identifies and separates these circuits of the contact system. The technique also pictures any cross-sectional area of the contact system and shows from which voxels the electricity flows through.

Moreover, it is found that as a cross-sectional slice of the resistor network model (for closed circuit) tends to the contact region, the total number of its resistors (slice asperities) increases. Furthermore, it is important to note that as a cross-sectional slice of the resistor network model (for both circuits, open/closed and closed) tends to the contact region, the total cross-sectional area of the cross-sectional slice decreases. This indicates that as the cross-sectional slice tends to the contact region, the total volume of its resistors (slice asperities) decreases.

The resistor network model is divided into three main regions where two regions have resistors connected in series. The third region is located between the other two regions, and its resistors are connected to a nontrivial fashion of parallel and series components. For the resistance across this region, an approach has been introduced by modifying the Greenwood's formula of total contact resistance. The sum of the total resistance in each region gives the total resistance across the resistor network model of the contact system.

References

[1] C. Roussos and J. Swingler, "The 3D nature of a real un-dismantled electrical contact interface," *Wear*, vols. 328–329, pp. 115–122, Apr. 2015.

[2] N. K. Myshkin, M. Braunovich, and V. V. Konchits, "The mechanics and tribophysics of electrical contacts," *J. Friction Wear*, vol. 36, no. 6, pp. 454–467, 2015.

[3] J. H. Kim, D. J. Srolovitz, P.-R. Cha, and J.-K. Yoon, "Capillarity and electromigration effects on asperity contact evolution in microelectromechanical systems switches," *J. Appl. Phys.*, vol. 100, no. 5, p. 054502, 2006.

[4] J. A. Greenwood, "Constriction resistance and the real area of contact," *J. Appl. Phys.*, vol. 17, no. 12, pp. 1621–1632, 1966.

[5] S. Gong, Z. H. Zhu, and E. I. Haddad, "Modeling electrical conductivity of nanocomposites by considering carbon nanotube deformation at nanotube junctions," *J. Appl. Phys.*, vol. 114, no. 7, p. 074303, 2013.

[6] S. Gupta, P. P. Manik, R. K. Mishra, A. Nainani, M. C. Abraham, and S. Lodha, "Contact resistivity reduction through interfacial layer doping in metal-interfacial layer-semiconductor contacts," *J. Appl. Phys.*, vol. 113, no. 23, p. 234505, Jun. 2013.

[7] F. A. Chaves, D. Jiménez, A. W. Cummings, and S. Roche, "Physical model of the contact resistivity of metal-graphene junctions," *J. Appl. Phys.*, vol. 115, no. 16, pp. 164513-1–164513-8, Apr. 2014

[8] M. Braunovic, N. K. Myshkin, and V. V. Konchits, "Fundamentals, applications and technology," in *Electrical Contacts*. New York, NY, USA: CRC Press, 2007.

[9] J. I. Goldstein, D. E. Newbury, D. C. Joy, C. E. Lyman, P. Echlin, and E. Lifshin, *Scanning Electron Microscopy and X-Ray Microanalysis*, 3rd ed. New York, NY, USA: Springer, 2003.

[10] J. Swingler and A. Lalechos, "Visualization and size distribution of contact spots at a real un-dismantled electrical contact interface," *J. Phys. D, Appl. Phys.*, vol. 42, no. 8, pp. 085304–085310, 2009.

[11] J. Swingler, "Clustering and the spatial distribution of contact spots at a real un-dismantled electrical contact interface," *J. Phys. D, Appl. Phys.*, vol. 43, no. 14, pp. 145302–145307, 2010.

[12] C. Roussos and J. Swingler, "Evaluation of electrical contacts using an X-Ray CT 3D visualisation technique," in *Proc. 27th Int. Conf. Electr. Contacts (ICEC)*, Dresden, Germany, Jun. 2014, pp. 326–331.

[13] W. Zhu, Y. Tian, X. Gao, and L. Jiang, "A method to measure internal contact angle in opaque systems by magnetic resonance imaging," *ACS J. Surf. Colloids*, vol. 29, no. 29, pp. 9057–9062, 2013.

[14] J. E. Johnson, T. E. McIffb, P. Leec, E. B. Tobyb, and K. J. Fischera, "Validation of radiocarpal joint contact models based on images from a clinical MRI scanner," *Comput. Methods Biomech. Biomed. Eng.*, vol. 17, no. 4, pp. 378–387, 2014.

[15] V. A. Popovich, W. Verwaal, M. Janssen, I. J. Bennett, and I. M. Richardson, "Application of X-ray computed tomography in silicon solar cells," in *Proc. 35th IEEE Photovoltaic Specialists Conf. (PVSC)*, Honolulu, HI, USA, Jun. 2010, pp. 1759–1764.

[16] C. W. Green, J. Farone, J. K. Briley, R. B. Eldridge, R. A. Ketcham, and B. Nightingale, "Novel application of X-ray computed tomography: Determination of gas/liquid contact area and liquid holdup in structured packing," *Ind. Eng. Chem. Res.*, vol. 46, no. 17, pp. 5734–5753, 2007.

[17] C. Roussos and J. Swingler, "Visualisation and characterisation of electrical contact spots for different current values using an X-Ray computer tomography," in *Proc. 12th Int. Conf. Comput. Methods Experim. Surf. Contact Mech. Including Tribol.*, Valencia, Spain, Apr. 2015, pp. 59–69.

[18] C. C. Roussos and J. Swingler, "Calculation of the electrical parameters from 3D visualisation data of non-disassembled contact interfaces," in *Proc. 61st IEEE Holm Conf. Electr. Contacts*, San Diego, CA, USA, Oct. 2015, pp. 82–89.

[19] A. V. Lalechos, J. Swingler, and J. Crane, "Visualisation of the contact area for different contact forces using X-ray computer tomography," in *Proc. 54th IEEE Holm Conf. Electr. Contacts*, Orlando, FL, USA, Oct. 2008, pp. 263–269.

[20] J. Swingler, "The resolution dependence of measured fractal characteristics for a real un-dismantled electrical contact interface," *Wear*, vol. 268, pp. 1178–1183, Mar. 2010.

[21] M. Ciavarella, G. Demelio, J. R. Barber, and Y. H. Jang, "Linear elastic contact of the Weierstrass profile," *Proc. Roy. Soc. London Ser. A*, vol. 456, pp. 387–405, Feb. 2000.

[22] W. R. Smythe, *Static and Dynamic Electricity*. New York, NY, USA: McGraw-Hill, 1950.

[23] P. van Dijk, "Critical aspects of electrical connector contacts," in *Proc. 2nd Int. Conf. Rel. Elect. Products Elect. Contacts (ICREPEC)*, Xiamen, China, Sep. 2007, pp. 161–168.

[24] M. D. Bryant, "Resistance buildup in electrical connectors due to fretting corrosion of rough surfaces," *IEEE Trans. Compon., Packag., Manuf. Technol. A*, vol. 17, no. 1, pp. 86–95, Mar. 1994.

[25] T. S. N. S. Narayanan, Y. W. Park, and K. Y. Lee, "Fretting corrosion of lubricated tin-plated contacts," *Ind. Lubrication Tribol.*, vol. 60, no. 5, pp. 233–241, 2008.

Constantinos C. Roussos received the B.Eng. (Hons.) degree in electrical and electronic engineering (sustainable energy systems) and the Ph.D. degree from Heriot-Watt University, Edinburgh, U.K., in 2012 and 2016, respectively, focused on the visualization and evaluation of electrical contact spots and asperities of a given contact system using X-ray computed tomography.

He is currently a Post-Doctoral Fellow of Concentrated Solar Power for the Energy with the Environment and Water Research Center, The Cyprus Institute, Nicosia, Cyprus.

Jonathan Swingler received the Joint B.Sc. (Hons.) degree in physics and chemistry from Keele University, Keele, U.K., in 1990, and the Ph.D. degree from Loughborough University, Loughborough, U.K., focused on the degradation of electrical contacts.

He was with the University of Southampton, Southampton, U.K., where he was involved in the physics of degradation and reliability of electrical/electronic materials and devices. He is currently an Associate Professor of Energy, Heriot-Watt University, Edinburgh, U.K, where he is developing reliability engineering science in connection with energy systems.

Dr. Swingler is a Fellow of the Institute of Physics.